(4*S*)-4-(3-^{18}F-Fluoropropyl)-L-Glutamate for Imaging of x_C^- Transporter Activity in Hepatocellular Carcinoma Using PET: Preclinical and Exploratory Clinical Studies

Sora Baek*[1], Andre Mueller*[2], Young-Suk Lim[3], Han Chu Lee[3], Young-Joo Lee[4], Gyungyub Gong[5], Jae Seung Kim[1], Jin-Sook Ryu[1], Seung Jun Oh[1], Seung Jin Lee[6], Claudia Bacher-Stier[2], Lüder Fels[2], Norman Koglin[2], Christoph A. Schatz[2], Ludger M. Dinkelborg[7], and Dae Hyuk Moon[1]

[1]*Department of Nuclear Medicine, Asan Medical Center, University of Ulsan College of Medicine, Seoul, Republic of Korea;* [2]*Bayer Pharma AG, Bayer Healthcare Pharmaceuticals, Berlin, Germany;* [3]*Department of Gastoenterology, Asan Medical Center, University of Ulsan College of Medicine, Seoul, Republic of Korea;* [4]*Department of Surgery, Asan Medical Center, University of Ulsan College of Medicine, Seoul, Republic of Korea;* [5]*Department of Pathology, Asan Medical Center, University of Ulsan College of Medicine, Seoul, Republic of Korea;* [6]*Asan Institute for Life Sciences, Asan Medical Center, University of Ulsan College of Medicine, Seoul, Republic of Korea; and* [7]*Piramal Imaging, Berlin, Germany*

(4*S*)-4-(3-^{18}F-fluoropropyl)-L-glutamate (^{18}F-FSPG, or BAY 94-9392) is a new tracer to assess system x_C^- transporter activity with PET. The aim of this study was to explore the tumor detection rate of ^{18}F-FSPG, compared with that of ^{18}F-FDG, in patients with hepatocellular carcinoma (HCC). **Methods:** Preclinically, in vivo HCC models of orthotopically implanted Huh7 and MH3924a cancer cells were studied with ^{18}F-FSPG in Naval Medical Research Institute nude mice ($n = 3$) and August-Copenhagen Irish rats ($n = 4$), respectively. Clinically, 5 patients with HCC who had hyper- or isometabolic lesions on ^{18}F-FDG PET were enrolled for evaluation of the tracer. Dynamic whole-body PET images with ^{18}F-FSPG were acquired for up to 120 min after injection of approximately 300 MBq of ^{18}F-FSPG. Immunohistochemical expression levels of the xCT subunit of the system x_C^- and CD44 of HCC were studied in 4 patients with HCC. **Results:** Strong tumor uptake and low background from nontarget tissue allowed excellent tumor visualization in animal models with orthotopically implanted liver tumors. ^{18}F-FSPG PET procedures were well tolerated in all patients. ^{18}F-FSPG PET and ^{18}F-FDG detected lesions in 5 of 5 and 3 of 5 patients, respectively. The maximal standardized uptake values (SUV) were comparable (^{18}F-FSPG, 4.7 ± 3.2; ^{18}F-FDG, 6.1 ± 2.9). The ratios of maximal SUV of the tumor to mean SUV of normal liver were also comparable (^{18}F-FSPG, 3.6 ± 2.2; ^{18}F-FDG, 2.7 ± 1.3), but the mean SUV of normal liver of ^{18}F-FSPG was significantly lower than that of ^{18}F-FDG ($P < 0.05$). Two patients with HCC who showed both xCT and CD44 expression had moderate or intense accumulation of ^{18}F-FSPG, but the remaining 2 patients with negative CD44 expression showed mild uptake. **Conclusion:** ^{18}F-FSPG was successfully translated from preclinical evaluation into patients with HCC. ^{18}F-FSPG may be a promising tumor PET agent with a high cancer detection rate in patients with HCC.

Key Words: glutamate; x_C^- transporter; positron emission tomography; hepatocellular carcinoma; ^{18}F-fluorodeoxyglucose

J Nucl Med 2013; 54:117–123
DOI: 10.2967/jnumed.112.108704

Hepatocellular carcinoma (HCC) is the sixth most common malignancy worldwide (*1*). Diagnosis is usually made by imaging studies, including dynamic CT or dynamic MRI (*2*). However, CT or MRI does not always show typical patterns, and a tumor biopsy may be needed for final diagnosis (*3*). PET with ^{18}F-FDG is not considered to be adequate for the diagnosis and staging of HCC (*4*). No other functional imaging with PET has been shown beneficial in predicting or monitoring the response to treatment.

(4*S*)-4-(3-^{18}F-fluoropropyl)-L-glutamate (BAY 94-9392, herein referred to as ^{18}F-FSPG) is a new ^{18}F-labeled L-glutamate derivative being taken up by the system x_C^- (*5*). The system x_C^- is a sodium-independent transporter that mediates the cellular uptake of cystine in exchange for intracellular glutamate at the plasma membrane (*6*). Intracellularly, cystine is reduced to 2 molecules of cysteine, which is used for glutathione synthesis. The system x_C^- does not discriminate between its natural substrate cystine and glutamate for the inward transport (*7*). Specific transport, retention, and no intracellular metabolism of ^{18}F-FSPG, a glutamate analog, via the system x_C^- were demonstrated (*5*). We recently reported the first, to our knowledge, clinical results of ^{18}F-FSPG in patients with non–small cell lung or breast cancer (*8*). System x_C^- is an important component of the tumor cell defense machinery against oxidative stress by providing a precursor for thiol-containing molecules. Thiol-containing molecules, such as the amino acid cysteine

Received May 12, 2012; revision accepted Aug. 6, 2012.
For correspondence or reprints contact: Dae Hyuk Moon, Department of Nuclear Medicine, Asan Medical Center, University of Ulsan College of Medicine, 88, Olympic-ro 43-gil, Songpa-gu, Seoul 138-736, Republic of Korea.
E-mail: dhmoon@amc.seoul.kr
*Contributed equally to this work.
Published online Dec. 11, 2012.

and the tripeptide glutathione, are major cellular components for the detoxification of reactive oxygen species and other electrophiles, including some chemotherapeutics (*9,10*). A continuous supply of glutathione and its precursors is critical for cell survival and provides a selective advantage for tumor growth (*11*). An increased expression and activity of system x_C^- potentially provides a survival advantage by enabling access to cysteine via the extracellularly more abundant cystine. Recently, it was reported that a splice variant of CD44, CD44v, stabilizes the xCT subunit of system x_C^- at the cell membrane, promoting its proper function (*12*).

The primary objectives of the current study were to explore tumor detection by ^{18}F-FSPG in animal models of HCC and to assess the tumor detection rate of ^{18}F-FSPG PET in patients with HCC. The secondary objectives were to perform quantitative analyses of ^{18}F-FSPG uptake in tumors and normal organs and to assess the safety and tolerability of ^{18}F-FSPG PET. Moreover, we evaluated the protein expression of xCT and CD44 by immunohistochemistry to explore the correlation with ^{18}F-FSPG uptake.

MATERIALS AND METHODS

Radiopharmaceutical Preparation

^{18}F-FSPG was radiolabeled as described previously (*5*). The investigational medicinal product ^{18}F-FSPG for the patient study was batch-manufactured at Asan Medical Center with an automated module (Modular Lab System; Eckert & Ziegler). Each batch met the criteria listed in the specification for clarity, identity, purity, radioactive concentration, specific activity, pH, bacterial endotoxin level, and sterility. The final product was formulated for intravenous injection with a drug substance per injected unit of 300 ± 30 MBq and 100 μg or less of tracer mass and a specific activity of 18.2 GBq/μmol or more. The decay-corrected radiochemical yield was 28.6% ± 12.9% (range, 11.2%−44.8%), and the radiochemical purity was 91.8% ± 1.5% (range, 90.8%−94.3%).

In Vivo Animal Studies

Animal experiments were performed at Bayer Pharma AG in compliance with the current version of the German law concerning animal protection and welfare. The protocol was approved by the Institutional and Regional Animal Care and Use Committee. All animals used in the studies were kept under normal laboratory conditions at a temperature of 22°C ± 2°C and a dark–light rhythm of 12 h. The acclimation period was at least 7 d before the beginning of the studies. During this period, animals were examined daily to verify the absence of abnormal signs.

Huh7 liver cancer cells were obtained from the Japanese Collection of Research Bioresources, and MH3924a cells from Cell Line Services. Naval Medical Research Institute nude (NMRI-*nu/nu*) mice (Charles River) (female; age, 5−6 wk; weight, 20−25 g) were inoculated by orthotopic injection of 2×10^6 human Huh7 liver cancer cells in a volume of 20 μL of Matrigel (BD Biosciences) plus medium without fetal calf serum. A small incision (1 cm) to the right of the linea alba was made, and the tumor cell suspension was injected into the left liver lobe. Wounds were closed using suture clips. PET studies with tumor-bearing mice were performed 12 d after tumor cell inoculation ($n = 3$). Three mice were injected with 125−170 μL of tracer solution containing an activity of 7.9−8.3 MBq of ^{18}F-FSPG. The PET scan was started 50 min after injection and continued for 20 min, followed by CT scanning for 10 min.

August-Copenhagen Irish (ACI) rats (Harlan Laboratories; female; mean weight, 150 g) were inoculated 9 d before the PET study by intrahepatic injection of 3×10^6 syngeneic Morris hepatoma MH3924a cells in a volume of 50 μL of Matrigel plus medium without fetal calf serum into the left liver lobe. PET studies with tumor-bearing rats were performed 9 d after tumor cell inoculation ($n = 4$). After the intravenous injection of 7.9−9.1 MBq of ^{18}F-FSPG, animals were subjected to the PET scan (tracer distribution period, 60 min). PET was performed for 10 min.

All animal imaging studies were performed with a small-animal PET/CT scanner (Inveon PET; Siemens AG). Regions of interest were drawn over the tumor and normal liver, and an average value within the region of interest was generated. The results of the region-of-interest analysis were reported as the percentage injected dose per gram of tissue (%ID/g).

Exploratory Clinical Study Design

An open-label, nonrandomized, single-dose explorative study was performed to evaluate the safety, tolerability, and diagnostic performance of ^{18}F-FSPG PET/CT in patients with HCC. The trial was registered at http://www.clinicaltrial.gov as NCT01103310. The primary outcome measure was the visual assessment of the tumor detection rate with ^{18}F-FSPG, compared with that of ^{18}F-FDG. The secondary outcome measures were quantitative analysis of ^{18}F-FSPG uptake in tumors and assessment of safety variables including vital signs, laboratory findings, electrocardiogram, and adverse events. The study protocol was approved by both the Institutional Review Board of Asan Medical Center and the Korea Food and Drug Administration. This study was conducted in accordance with the Helsinki Declaration. Investigators disclosed potential conflicts to study participants. All patients provided written informed consent before participation in the study.

Patients

Patients were enrolled if they had HCC, ranged in age from 35 to 75 y, and had an ^{18}F-FDG PET/CT scan that showed an iso- to hypermetabolic or heterogeneous metabolic liver lesion. Other inclusion criteria were an interval between ^{18}F-FDG and ^{18}F-FSPG PET/CT of 4 wk or less, adequate recovery (excluding alopecia) from potential previous anticancer treatment, an Eastern Cooperative Oncology Group performance status of 0–2, and adequate function of major organs. No chemotherapy, radiotherapy, or immune–biologic therapy or biopsy was allowed between the ^{18}F-FDG and ^{18}F-FSPG PET/CT scans. The patient had to have histologic confirmation of the tumor. However, histologic diagnosis of HCC was not necessary if the nodule was larger than 2 cm and if 2 dynamic imaging studies using contrast agents showed arterial hyperenhancement and washout in the venous phase. Patients were excluded from the study if any of the following conditions applied to them: being pregnant or lactating; having a concurrent, severe, or uncontrolled or unstable medical disease other than cancer; having a lifetime history of alcohol or drug abuse; being a relative or student of the investigator or otherwise dependent; or participating or having participated in another clinical study involving the administration of an investigational drug during the preceding 4 wk. Patients were recruited by referral from investigators.

PET/CT Procedure

^{18}F-FDG and ^{18}F-FSPG PET/CT images were obtained with a PET/CT scanner (Biograph True Point 40; Siemens). ^{18}F-FDG PET/CT was performed for clinical reasons as described previously

(*13*). ^{18}F-FSPG PET/CT studies were performed during 3 time intervals (the first interval was from 0 to 45 min, the second was from 60 to 75 min, and the third was from 105 to 120 min). During each interval, 1 low-dose CT scan (80 kV, 31 mAs, CARE Dose4D; Siemens) without contrast medium administration was recorded for attenuation correction of the PET scan. Five consecutive images from the skull base to mid thigh were acquired for the first imaging interval of 0−45 min along with the injection of 300 ± 10 MBq of ^{18}F-FSPG as follows: 30 s, 30 s, 1 min, 2 min, and 2 min per bed position. During the second and third imaging intervals, 1 image of the skull base to mid thigh was acquired per imaging interval with the same acquisition parameters as were applied for the previous scan.

Patients were asked to void their urinary bladder immediately after the first scan. Urinary bladder voiding was also encouraged before and after the second and third imaging sessions. Effective radiation doses for ^{18}F-FSPG as extrapolated from biodistribution studies in mice to humans were 5.10 mSv for a male and 6.5 mSv for a female subject. The total radiation exposure from the 3 CT examinations did not exceed 3 mSv. Emission data were reconstructed by means of the Siemens TrueX reconstruction with 3 iterations and 21 subsets. No correction for partial-volume effects was performed.

Image Analysis of Clinical PET Studies

The PET/CT studies were assessed visually by the consensus of 2 board-certified nuclear medicine physicians who were informed of all available clinical and laboratory findings. The CT scans were assessed for the exact location of HCC lesions. For dynamic assessment of ^{18}F-FSPG uptake, a spheric volume of interest with a diameter of 1.2 cm was placed on tumor, and a spheric volume of interest with a diameter of 1.5 cm was placed on the pancreas and kidneys. Volumes of interest on normal liver tissue and descending thoracic aorta (as the blood pool) were drawn as previously recommended (*14*). Mean standardized uptake value (SUVmean) of the volume of interest were obtained on each time frame to generate a time–activity profile of the ^{18}F-FSPG uptake. All standardized uptake values (SUVs) were normalized to the injected dose and the patients' body weight and were defined as follows:

$$\text{SUV} = \text{activity (Bq/g)}/(\text{injected activity [Bq]}/\text{body weight [g]}).$$

The ^{18}F-FSPG PET/CT image acquired 60 min after injection was used for visual and quantitative analysis. The number, location, size, and intensity of all abnormal uptake values were described relative to the background uptake in normal comparable tissues. Intensity features were classified as absent, minor, or major accumulation. Mildly increased uptake higher than that of the background was defined as minor accumulation. Moderately or markedly increased uptake, compared with the background, was considered major accumulation. Lesions with minor or major accumulation were regarded as positive. Selected lesions were visually compared with the uptake of ^{18}F-FDG. A 3-step score was applied: visibility with ^{18}F-FSPG was lower than, as good as, or better than that in the ^{18}F-FDG PET image. The maximal standardized uptake value (SUVmax) of each selected tumor lesion was measured using the single maximum pixel count within the lesion. The SUV ratio (SUVR) was obtained by calculating the ratio of the SUVmax of the tumor lesion to the SUVmean of normal liver.

Safety Monitoring

Adverse events were continuously recorded, beginning with patient enrolment until the last patient contact on days 3–8 after ^{18}F-FSPG administration. The safety of ^{18}F-FSPG was assessed using blood parameters (hematology, clotting status, serum chemistry), semiquantitative urine dip-stick measurements, vital signs, electrocardiograms, and physical examinations at baseline and at about 2 and 24 h after the intravenous administration of ^{18}F-FSPG.

Immunohistochemistry of x_C^- Transporter and CD44

Tumor tissues obtained during surgery for routine diagnostic pathologic examinations were used for immunohistochemistry studies of the xCT subunit of system x_C^- and CD44. Formalin-fixed, paraffin-embedded tissue sections were immunohistochemically stained for xCT and CD44 with a Benchmark automatic immunostaining device (Ventana Medical Systems). Five-micrometer-thick sections, obtained with a microtome, were transferred onto adhesive slides and dried at 62°C for 30 min. After incubation with primary antibodies against the xCT subunit (1:250 dilution; NB300-318, polyclonal antixCT antibody [Novus Biologicals]) and CD44 (1:100 dilution; Clone DF 1485 [DakoCytomation]), the slides were incubated using a biotinylated, anti-mouse secondary antibody. Then, antigens were detected using peroxidase-labeled streptavidin, a streptavidin–biotin kit, and the 3,3′-diaminobenzidine chromogen as a substrate. The level of xCT and CD44 was examined by an experienced pathologist who was completely masked to any patient and imaging information. The results of the immunoassay for xCT and CD44 were semiquantitatively assessed on a scale of 0, 1 (weak), 2 (medium), or 3 (strong), with a sample being reported as positive if more than 10% of the cells in the sample were positively stained.

Statistical Analysis

Data were reported as the mean ± SD unless otherwise specified. A P value of less than 0.05 was considered to be statistically significant. Quantitative parameters were compared using the Mann–Whitney U test. All statistical tests were performed with SPSS Statistics (version 19; SPSS, Inc., IBM Co.) for Windows (Microsoft).

RESULTS

PET of ^{18}F-FSPG in Animals Bearing Liver Tumors

Huh7 tumors in the liver of NMRI-*nu/nu* mice and syngeneic MH3924a tumors in ACI rats were well visualized by PET with ^{18}F-FSPG (Fig. 1). A fast clearance of radioactivity from the normal liver and all other organs was observed, resulting in a low background signal. In addition to the activity in the kidneys and the bladder as excretion organs, only the pancreas and thymus were visible. Uptake values of 4.4 ± 1.3 %ID/g (n = 3) at 60 min after injection were determined in the orthotopically implanted Huh7 tumor cell lesions. Background uptake in normal liver was 0.4 ± 0.1 %ID/g, resulting in a tumor-to-background ratio of 11 ± 1.3. Uptake values of 1.5 ± 0.4 %ID/g at 60 min after injection were observed in MH3924a tumors, which were higher than those of the normal liver in all rats (0.5 ± 0.2 %ID/g).

Radiopharmaceutical Synthesis and Dose Administered for Clinical Studies

The specific activity of ^{18}F-FSPG at the time of synthesis was 65.3 ± 15.6 GBq/μmol (range, 46.8−87.0 GBq/μmol). The mean administered activity was 304.1 ± 9.6 MBq (range, 292.3−318.2 MBq), and the mean administered mass dose was 2.9 ± 0.8 μg (range, 2.2−4.3 μg).

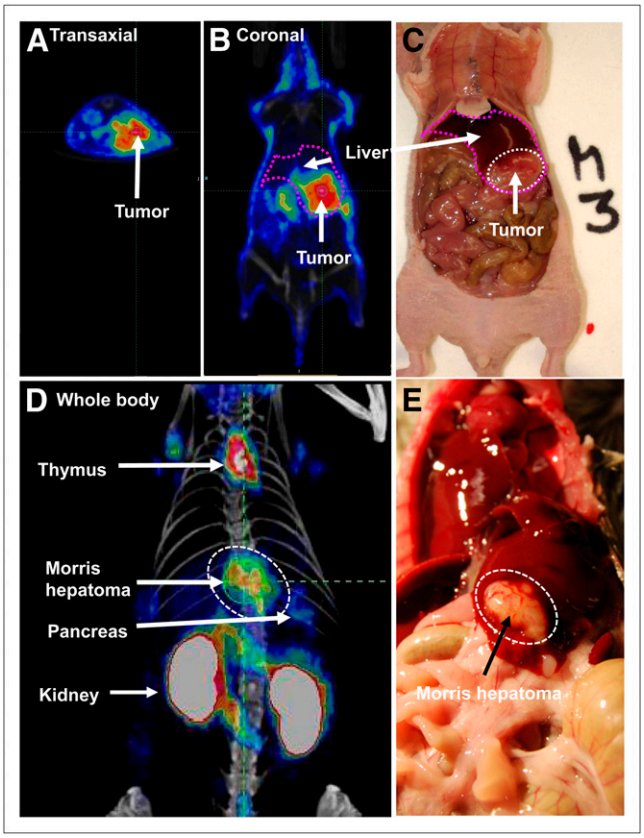

FIGURE 1. ^{18}F-FSPG PET in animals bearing orthotopically implanted liver tumors. Transaxial (A) and coronal images (B) of NMRI-*nu/nu* mouse bearing orthotopically implanted human Huh7 tumor cells obtained 60 min after injection of ^{18}F-FSPG shows high activity in liver tumor. Photographic image of same animal demonstrates extent of tumor tissue, which correlates with PET signal (C). Maximum-intensity projection of MH3924a tumors (dotted circle) in ACI rats shows strong tumor signal and low background. In addition, kidneys, pancreas, and thymus are visible (D). Photographic image of same animal shows good correlation of tumor (dotted circle) with extent and location of ^{18}F-FSPG uptake (E).

Patients and ^{18}F-FSPG PET/CT Procedure

Five patients with newly diagnosed HCC were enrolled in this study and were examined between December 2010 and February 2011 (5 men; age range, 60−71 y). All patients who agreed to participate completed the study. The patient and lesion characteristics are listed in Table 1. Four patients were diagnosed as having HCC by histologic confirmation, but 1 patient was diagnosed on the basis of the lesion size and typical patterns on dynamic imaging studies using contrast agents (patient 5). The American Joint Committee on Cancer TNM staging was T1N0M0 in all patients. No patient had prior radiation or chemotherapy. All patients were positive for viral hepatitis B antigen. The mean time interval between ^{18}F-FDG and ^{18}F-FSPG PET/CT was 3.8 ± 3.3 d (range, 1−9 d). ^{18}F-FSPG PET/CT studies were well tolerated by all patients and were completed without any scanner- or patient-related problems. All ^{18}F-FSPG PET/CT procedures were performed as planned. Surgery was performed after the PET study in 4 patients. The mean time interval between ^{18}F-FSPG PET/CT and surgery was 4.5 ± 3.4 d.

Safety

The administration of the ^{18}F-FSPG and the PET/CT procedures were well tolerated by all 5 patients. No clinically relevant changes in safety parameters were observed. There were no study drug–related adverse events.

Biodistribution of ^{18}F-FSPG in Patients with HCC

The overall image quality was sufficient for diagnosis in all patients. Defluorination of the tracer, which would result in bone uptake of free ^{18}F-fluoride, was not observed. Figure 2 shows the biodistribution of ^{18}F-FSPG over 105 min. ^{18}F-FSPG showed high uptake in the kidney, bladder, and pancreas. The pancreas activity increased continuously, plateauing at 60 min after injection (SUVmean, 11.8 ± 2.5). Blood-pool activity cleared rapidly (SUVmean, 0.8 ± 0.2 at 60 min after injection). No focal or elevated uptake was observed in the brain, muscle, small or large intestinal track, or the cortical or trabecular bone surfaces. The liver showed an initial decrease followed by prolonged uptake, which resulted in normal visualization on delayed images (SUVmean, 1.3 ± 0.3 at 60 min after injection). There were large variations in tumor uptake. The mean value slowly decreased continuously (SUVmean, 3.5 ± 2.4 at 60 min after injection), but the tumor-to-liver ratios increased over time up to 60 min (tumor-to-liver ratio of SUVmean, 2.7 ± 1.6 at 60 min) because of the clearance of the background liver activity over time. The tumor-to-blood ratio of SUVmean increased up to 105 min because of rapid blood clearance (4.7 ± 4.1 at 60 min and 6.9 ± 5.0 at 105 min after injection, $P < 0.05$).

Comparison of ^{18}F-FDG and ^{18}F-FSPG Uptake in HCC

Three patients with hypermetabolic and 2 patients with isometabolic lesions on ^{18}F-FDG PET were included. The results of the visual and quantitative analyses of ^{18}F-FSPG PET are summarized in Table 1. All patients had a single lesion. Three patients had minor accumulation (patients 1, 4, and 5), and 2 patients showed major uptake of ^{18}F-FSPG (patients 2 and 3). No additional lesion was detected on ^{18}F-FSPG PET/CT. Two isometabolic ^{18}F-FDG lesions (patients 1 and 5) were better visualized on ^{18}F-FSPG PET (for patient 1: Fig. 3, Supplemental Video 1 [supplemental materials are available online only at http://jnm.snmjournals.org], and Supplemental Fig. 1; and for patient 5: Supplemental Fig. 2), whereas the other 3 lesions (patients 2–4) showed similar intensities (for patient 2: Fig. 4, Supplemental Video 2, and Supplemental Fig. 3; for patient 3: Supplemental Fig. 4; and for patient 4: Supplemental Fig. 5). Therefore, the tumor detection rate with ^{18}F-FSPG by visual assessment was 100% (5/5), whereas that of ^{18}F-FDG was 60% (3/5). Patient 1 with isometabolic ^{18}F-FDG uptake had a small focus of increased ^{18}F-FSPG uptake in the central area of the tumor. The rest of the tumor was isometabolic on ^{18}F-FSPG PET.

TABLE 1
Demographics, Pathology, and PET Data of Study Population

Patient no.	Age (y)	Sex	Tumor size (cm)	Histologic grade	Visual ^{18}F-FSPG analysis*	SUVmax at 60 min		Immunohistochemistry score	
						^{18}F-FDG	^{18}F-FSPG	x_C^-	CD44
1	50	M	6.2	G1	Minor†‡	3.5	3.9‡	2	0
2	42	M	5.0	G2	Major§	10.0	10.4	1	2
3	52	M	6.0	G3	Major§	8.2	3.5	1	2
4	56	M	3.3	G2	Minor§	5.5	3.4	1	0
5	56	M	2.3	NA	Minor†	3.6	2.4	NA	NA

*Lesions with minor or major ^{18}F-FSPG accumulation were regarded as positive.
†Isometabolic ^{18}F-FDG uptake. Visually assessed intensity of ^{18}F-FSPG was better than that of ^{18}F-FDG.
‡^{18}F-FSPG uptake of small focus that is located in central area of tumor.
§Hypermetabolic ^{18}F-FDG uptake. Intensities of ^{18}F-FDG and ^{18}F-FSPG uptake were same.
NA = not assessed.

For comparison of quantitative values of ^{18}F-FSPG PET and ^{18}F-FDG, the SUVmax of the representative lesions at 60 min after injection of ^{18}F-FSPG was analyzed. The SUVmax and SUVR of HCC lesions were not significantly different, but the SUVmean of the liver of ^{18}F-FSPG was significantly lower than that of ^{18}F-FDG (Table 2, $P < 0.05$).

Comparison of ^{18}F-FSPG Uptake with Pathologic Tumor Grading and Immunohistochemistry

Among the 4 patients with pathologic results, 1 patient with well-differentiated HCC (patient 1) showed isometabolic ^{18}F-FDG and ^{18}F-FSPG uptake that was not differentiated from the normal liver (Fig. 3, Supplemental Video 1, and Supplemental Fig. 1). Interestingly, this patient showed a central small focus of mild ^{18}F-FSPG uptake. However, this lesion of central ^{18}F-FSPG uptake could not be localized for pathologic evaluation. Two patients with moderately differentiated HCC (patients 2 and 4) showed the same degree of ^{18}F-FDG and ^{18}F-FSPG uptake (for patient 2: Fig. 4, Supplemental Video 2, and Supplemental Fig. 3; and for patient 4: Supplemental Fig. 5). In 1 patient with poorly differentiated HCC, the tumor was better visualized using ^{18}F-FDG PET (patient 3: Supplemental Fig. 4).

Immunohistochemical staining of tumors revealed that all 4 patients had x_C^- transporter–positive tumors (3 with 1+ and 1 with 2+ immunostaining), but only 2 had CD44-positive tumors (patients 2 and 3) with 2+ score (Table 1). One patient with an xCT 2-positive but CD44-negative tumor (patient 1) showed a central focus of mild ^{18}F-FSPG

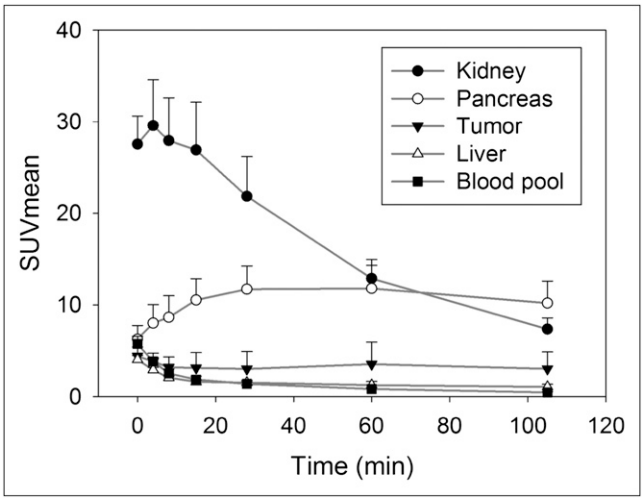

FIGURE 2. Mean and SD of SUVmean of ^{18}F-FSPG distribution as function of time. Pancreas activity increases continuously, plateauing at approximately 15−60 min. Kidney and remaining body activity decrease over time. Tracer in tumors shows rapid accumulation, followed by plateau phase, with minimal decrease of activity until 60 min after injection.

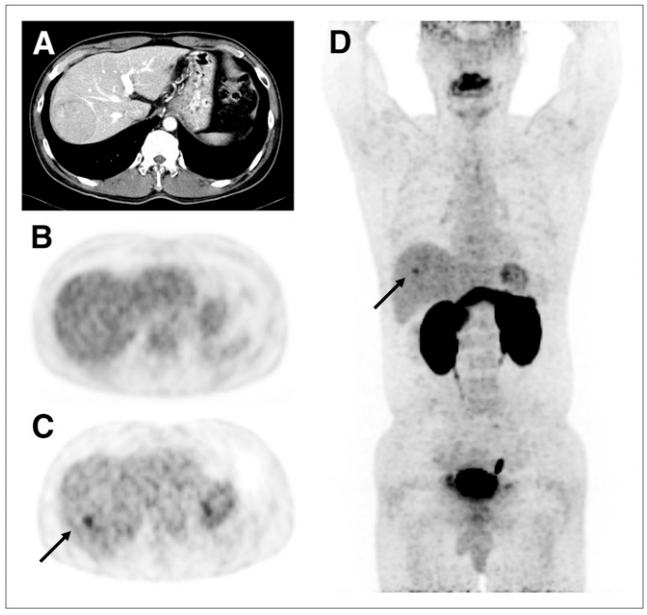

FIGURE 3. A 50-y-old man with well-differentiated HCC (patient 1). Transverse CT image with contrast enhancement shows hypervascular mass in right lobe (A). There is no significant uptake of ^{18}F-FDG in lesion, compared with surrounding noncancerous liver tissue (B). Transverse (C) and maximum-intensity-projection (D) ^{18}F-FSPG images show focal mildly increased uptake in center of mass (arrow), whereas rest of tumor is indistinguishable from surrounding noncancerous liver tissue.

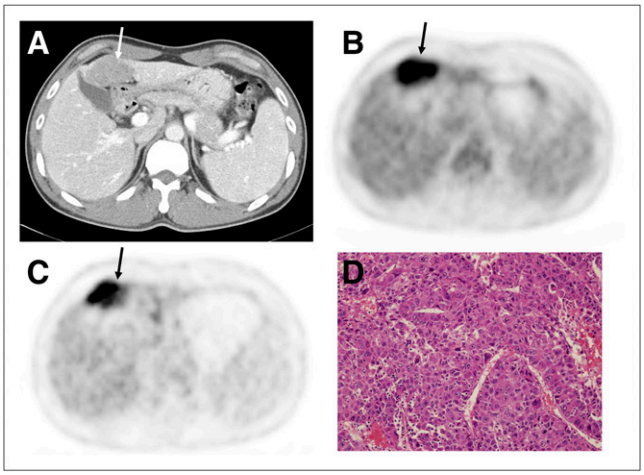

FIGURE 4. Transverse CT (A), ^{18}F-FDG (B), and ^{18}F-FSPG PET images (C) of 42-y-old man (patient 2) with moderately differentiated HCC (D, ×400) show mildly attenuated mass with markedly increased ^{18}F-FDG and ^{18}F-FSPG uptake in segment IV of liver (arrows).

uptake (SUVmax, 3.9; Fig. 3). Most tumor tissue had absent ^{18}F-FSPG uptake that was not differentiated from the normal liver (SUVmean, 1.8). Another patient with CD44-negative tumor tissue (patient 4) showed a minor accumulation (SUVmax, 3.4; SUVmean, 2.3). Two tumors with CD44 2-positive staining showed major accumulation of ^{18}F-FSPG uptake at 60 min (for patient 2: SUVmax, 10.4, and SUVmean, 7.7; for patient 3: SUVmax, 3.5, and SUVmean, 2.7).

DISCUSSION

Clear tumor visualization with low background signal from healthy liver and other tissues was observed preclinically in orthotopic HCC rodent models. ^{18}F-FSPG detected HCC lesions in all 5 patients, of whom 2 had isometabolic ^{18}F-FDG lesions. Rapid blood clearance without delayed bone uptake was observed. ^{18}F-FSPG PET/CT procedures were well tolerated by all 5 patients without any clinically relevant changes in safety parameters. Our findings suggest that ^{18}F-FSPG may be a promising tumor imaging agent with a high cancer detection rate in patients with HCC.

The biodistribution of ^{18}F-FSPG in rodents and humans showed a high pancreatic and renal uptake with rapid blood clearance that allowed tumor lesions to be imaged with good contrast. These data are consistent with previously reported data on ^{18}F-FSPG in non–small cell lung or breast cancer patients (*8*) and previous results of xCT protein distribution in the pancreas (*15*) and kidney (*16*). In cultured human pancreatic ductal cells, cystine uptake was also found to be mediated by x_C^- transporter (*17*). ^{18}F-FSPG uptake in rat thymus may likely be due to activated macrophages, dendritic cells, and fibroblasts that supply T cells with cysteine because T cells are unable to take up cystine and depend on extracellular cysteine (*18*). The average tumor-to-blood ratio increased up to 105 min because of rapid blood clearance. Our data suggest that the equilibrium condition is not achieved, and specific retention of ^{18}F-FSPG may be considered irreversible on the imaging timescale. Because the tumor-to-liver ratio increased over time up to 60 min, we selected ^{18}F-FSPG PET images at 60 min after injection to assess the x_C^- transporter status and compared them with ^{18}F-FDG images.

TABLE 2
Comparison of ^{18}F-FDG and ^{18}F-FSPG Uptake at 60 Minutes After Injection in Patients with HCC

Parameter	^{18}F-FDG	^{18}F-FSPG	*P*
Qualitative sensitivity	60% (3/5)	100% (5/5)	NS
Quantitative analysis			
SUVmax	6.2 ± 2.9	4.7 ± 3.2	NS
SUVmean of liver	1.9 ± 0.2	1.3 ± 0.3	<0.05
SUVR	2.7 ± 1.3	3.6 ± 2.2	NS

NS = not significant.

The main result of this study may be that ^{18}F-FSPG PET detected 2 HCC patients with isometabolic ^{18}F-FDG uptake. Three HCC patients with moderate or poor differentiation had hypermetabolic ^{18}F-FDG uptake, but 1 patient with well-differentiated HCC showed isometabolic ^{18}F-FDG uptake. Although in 1 patient well-differentiated HCC was detected, ^{18}F-FSPG uptake was limited to the central small area. The rest of the tumor lesion was not differentiated from the rest of the normal liver parenchyma (patient 1; Fig. 3). It is probable that the nature of the lesion of central high uptake in this patient may differ from that of the rest of the tumor. The other patient with isometabolic ^{18}F-FDG uptake did not undergo a biopsy of the lesion. However, the intensity of ^{18}F-FSPG uptake in these 2 HCCs with isometabolic ^{18}F-FDG was only minor. These findings suggest that ^{18}F-FSPG may have some difficulty in detecting well-differentiated HCC, although we obtained encouraging results, compared with ^{18}F-FDG in this study. A larger number of patients should be studied to assess the detection rate of ^{18}F-FSPG in relation to histologic differentiation.

We obtained tumor samples from surgery for immunohistochemical analysis of the xCT subunit of system x_C^- and CD44 expression to explore the potential correlation with ^{18}F-FSPG uptake. Because of the small number of samples studied ($n = 4$) and the observed heterogeneity of ^{18}F-FSPG PET (patient 1), our data are limited and it is difficult to draw any conclusions. However, our findings of the major accumulation of ^{18}F-FSPG in 2 tumors with both xCT and CD44 expression and minor ^{18}F-FSPG uptake in patients with negative CD44 but positive xCT may be consistent with the role of the CD44 splice variant in stabilizing the xCT subunit. System x_C^- expression was recently studied in patients with HCC (*19*). The expression of xCT was often elevated in these patients and was associated with poor prognosis. CD44 expression in HCC has been shown to be related to metastasis (*20*), survival (*21*), and chemoresponse (*22*). Future studies in a larger number of patients with HCC should be performed to validate whether ^{18}F-FSPG PET can assess system x_C^- activity

and to investigate the clinical significance of ^{18}F-FSPG PET in terms of indicating system x_C^- activity.

This study has several limitations. The high detection rate must be considered with caution because of the small number of included patients and large tumor size. Clearly, the promising sensitivity of ^{18}F-FSPG has to be examined in a larger patient cohort. Additionally, inclusion of patients based on the metabolic status of ^{18}F-FDG lesions may bias the diagnostic potential of ^{18}F-FSPG. Finally, we did not examine tumor heterogeneity. The potential heterogeneity of xCT or CD44 expression might have resulted in discordant imaging results. In particular, we have no information on the expression levels of xCT and CD44 in the lesion of central high uptake in patient 1. Tumor heterogeneity can lead to underestimation of the tumor landscape portrayed from single tumor-biopsy samples (*23*). We need to determine whether the heterogeneity detected by ^{18}F-FSPG PET provides more information on tumor biology.

CONCLUSION

^{18}F-FSPG may be a promising tumor imaging agent with a high cancer detection rate and favorable biodistribution in patients with HCC. More studies are needed to investigate the diagnostic value of this agent further in comparison with conventional imaging modalities. Correlation studies with underlying tumor biology including tumor progression, metastasis, and chemoresistance are needed to provide more insights into the potential clinical applications of ^{18}F-FSPG PET.

DISCLOSURE

The costs of publication of this article were defrayed in part by the payment of page charges. Therefore, and solely to indicate this fact, this article is hereby marked "advertisement" in accordance with 18 USC section 1734. This study was sponsored and financially supported by Bayer HealthCare. The role of Bayer HealthCare was in the design and performance of the study and in the provision of logistical support during the clinical trial. All clinical data were recorded and analyzed by Asan Medical Center. All authors had full access to the data. Bayer HealthCare was permitted to review the manuscript and suggest changes, but the final decision on content was exclusively retained by the authors. The authors had final responsibility for the decision to submit for publication. No other potential conflict of interest relevant to this article was reported.

ACKNOWLEDGMENTS

We thank all of the investigators who participated in this trial in the Nuclear Medicine Department of Asan Medical Center, especially Sae Jung Na, Seol Hoon Park, Kwang Ho Shin, Seon Hee Yoo, Sin Ae Kim, and Jung Eun Kim, for their support of the trial. We thank Woo Young Chung, Kyung Sik Kim, and Seung Yong Park for their excellent technical assistance, and the Cyclotron Team, particularly Sung Jae Lim, Woo Yeon Moon, Soo Jeong Lim, Dong Ryeol Lee, and Sang Ju Lee, for performing radiotracer synthesis. Additionally, we gratefully acknowledge the skillful technical assistance of the research staff at Bayer HealthCare, Berlin, for supporting the preclinical studies.

REFERENCES

1. Ferenci P, Fried M, Labrecque D, et al. World Gastroenterology Organisation Guideline. Hepatocellular carcinoma (HCC): a global perspective. *J Gastrointestin Liver Dis.* 2010;19:311–317.
2. Poon D, Anderson BO, Chen LT, et al. Management of hepatocellular carcinoma in Asia: consensus statement from the Asian Oncology Summit 2009. *Lancet Oncol.* 2009;10:1111–1118.
3. Jelic S, Sotiropoulos GC. Hepatocellular carcinoma: ESMO Clinical Practice Guidelines for diagnosis, treatment and follow-up. *Ann Oncol.* 2010;21(suppl 5):v59–v64.
4. Khan MA, Combs CS, Brunt EM, et al. Positron emission tomography scanning in the evaluation of hepatocellular carcinoma. *J Hepatol.* 2000;32:792–797.
5. Koglin N, Mueller A, Berndt M, et al. Specific PET imaging of xC- transporter activity using a ^{18}F-labeled glutamate derivative reveals a dominant pathway in tumor metabolism. *Clin Cancer Res.* 2011;17:6000–6011.
6. Bannai S. Exchange of cystine and glutamate across plasma membrane of human fibroblasts. *J Biol Chem.* 1986;261:2256–2263.
7. Patel SA, Warren BA, Rhoderick JF, Bridges RJ. Differentiation of substrate and non-substrate inhibitors of transport system xc(-): an obligate exchanger of L-glutamate and L-cystine. *Neuropharmacology.* 2004;46:273–284.
8. Baek S, Choi C, Ahn SH, et al. Exploratory clinical trial of (4S)-4-(3-[18F] fluoropropyl)-L-glutamate for imaging xC- transporter using positron emission tomography in patients with non-small cell lung or breast cancer. *Clin Cancer Res.* 2012;18;5427–5437.
9. Okuno S, Sato H, Kuriyama-Matsumura K, et al. Role of cystine transport in intracellular glutathione level and cisplatin resistance in human ovarian cancer cell lines. *Br J Cancer.* 2003;88:951–956.
10. Huang Y, Dai Z, Barbacioru C, Sadee W. Cystine-glutamate transporter SLC7A11 in cancer chemosensitivity and chemoresistance. *Cancer Res.* 2005;65:7446–7454.
11. Ogunrinu TA, Sontheimer H. Hypoxia increases the dependence of glioma cells on glutathione. *J Biol Chem.* 2010;285:37716–37724.
12. Ishimoto T, Nagano O, Yae T, et al. CD44 variant regulates redox status in cancer cells by stabilizing the xCT subunit of system xc(-) and thereby promotes tumor growth. *Cancer Cell.* 2011;19:387–400.
13. Yoon DH, Baek S, Choi CM, et al. FDG-PET as a potential tool for selecting patients with advanced non-small cell lung cancer who may be spared maintenance therapy after first-line chemotherapy. *Clin Cancer Res.* 2011;17:5093–5100.
14. Wahl RL, Jacene H, Kasamon Y, Lodge MA. From RECIST to PERCIST: Evolving Considerations for PET response criteria in solid tumors. *J Nucl Med.* 2009;50(suppl 1):122S–150S.
15. Bassi MT, Gasol E, Manzoni M, et al. Identification and characterisation of human xCT that co-expresses, with 4F2 heavy chain, the amino acid transport activity system xc. *Pflugers Arch.* 2001;442:286–296.
16. Burdo J, Dargusch R, Schubert D. Distribution of the cystine/glutamate antiporter system xc- in the brain, kidney, and duodenum. *J Histochem Cytochem.* 2006;54:549–557.
17. Sweiry JH, Sastre J, Vina J, Elsasser HP, Mann GE. A role for gamma-glutamyl transpeptidase and the amino acid transport system xc- in cystine transport by a human pancreatic duct cell line. *J Physiol.* 1995;485:167–177.
18. Edinger AL, Thompson CB. Antigen-presenting cells control T cell proliferation by regulating amino acid availability. *Proc Natl Acad Sci USA.* 2002;99:1107–1109.
19. Guo W, Zhao Y, Zhang Z, et al. Disruption of xCT inhibits cell growth via the ROS/autophagy pathway in hepatocellular carcinoma. *Cancer Lett.* 2011;312:55–61.
20. Hou Y, Zou Q, Ge R, Shen F, Wang Y. The critical role of CD133(+)CD44 (+/high) tumor cells in hematogenous metastasis of liver cancers. *Cell Res.* 2012;22:259–272.
21. Endo K, Terada T. Protein expression of CD44 (standard and variant isoforms) in hepatocellular carcinoma: relationships with tumor grade, clinicopathologic parameters, p53 expression, and patient survival. *J Hepatol.* 2000; 32:78–84.
22. You H, Ding W, Dang H, Jiang Y, Rountree CB. c-Met represents a potential therapeutic target for personalized treatment in hepatocellular carcinoma. *Hepatology.* 2011;54:879–889.
23. Gerlinger M, Rowan AJ, Horswell S, et al. Intratumor heterogeneity and branched evolution revealed by multiregion sequencing. *N Engl J Med.* 2012;366:883–892.